HYTEC INCORPORATED

Summary Report for PHENIX Silicon/Pixel Detector Concept Study

William O. Miller, Steve Ney, and Roger Smith
12/31/2002

	Name:	Phone & E-Mail	Signature:
Main Author:	Steve Ney & William O. Miller	505.661.3000 ext. 23 ney@hytecinc.com	Stephen Ney
Approved:	Steve Ney	505.661.3000 ext. 23 ney@hytecinc.com	Stephen Ney

Abstract

The PHENIX experiment at Brookhaven Laboratories has been very successful in unlocking the mysteries behind heavy-ion reactions in high-energy physics. Further work remains however in spin physics, pp physics, gluon structure functions, and early, highest energy-density stage of heavy-ion reactions. These areas of potential study can only be accomplished with an addition of a silicon/pixel detector to the PHENIX experiment. This report summarizes a concept study for the structure and cooling of the silicon/pixel detector. The report identifies the research and development areas still needing further study to complete the design of the detector and gives a rough cost estimate required to bring the detector to final design.

Design Engineering
Advanced Composite Applications
Ultra-Stable Platforms

110 Eastgate Dr.
Los Alamos, NM 87544

Phone 505 661-3000
Fax 505 662-5179
www.hytecinc.com

PHENIX

Revision Log

Rev.	Date	Author(s)	Summary of Revisions/Comments
O.I.	01/13/2003	S. Ney & W.O. Miller	Initial release.

Table of Contents

1. Definitions

2D	Two-Dimensional
3D	Three-Dimensional
C-C	Carbon-Carbon
CTE	Coefficient of Thermal Expansion
FE	Finite Element
FEA	Finite Element Analysis
FTE	Full Time Employee
GFRP	Graphite Fiber Reinforced Plastic
HBD	Hadron Blind Detector
HEP	High Energy Physics
ID	Inner Diameter
LHC	Large Hadron Collider
RL	Radiation Length
SSC	Superconducting Super Collider
SSD	Silicon Strip Detector
TPC	Time Projection Chamber

2. Concept Study Requirements

The basic requirements for the PHENIX tracker are given in the outline below.

1. Clamshell Design:
    i. Separates into two halves along the vertical axis
2. Detector Coverage:
    i. Hermeticity: single overlap circumferentially
    ii. 160^o coverage in each half of barrel section
    iii. 4 layers of pixels and/or strip detectors in barrel section
    iv. 180^o coverage in each half of the end cap sections
    v. 4 layers of pixel detectors in end cap sections
3. +/- 40^o Envelop for HBD/TPC maintained around barrel section

   i. End cap pixel disks, utilities, and barrel detector end support are outside of envelope
   ii. Main clamshell support structure is inside of envelop, but less than 0.5% RL
4. RL of 1% or less for each detector layer (includes: detectors, structure, and utilities)
5. Dimensional and structural stability of less than 25 μm for detectors and 100 μm gravitational structural stability of entire tracker
6. Utility Routing:
   i. Along barrel end support for barrel region
   ii. Radial at pole tips for the end caps
7. Mounting of Tracker:
   i. Off of magnet pole tips
   ii. Tracker to behave as a rigid body structure
   iii. Operating Temperature: Room temperature (or possibly 0^{o} option?)

3. PHENIX Silicon/Pixel Detector Description

The PHENIX silicon/pixel detector is split into three regions of detectors, a center region and two end cap regions. The center region consists of four-barrel type layers of either silicon or pixel detectors. Figure 3.1-1 shows the layout of the layers with the types of detectors to be used in each layer defined.

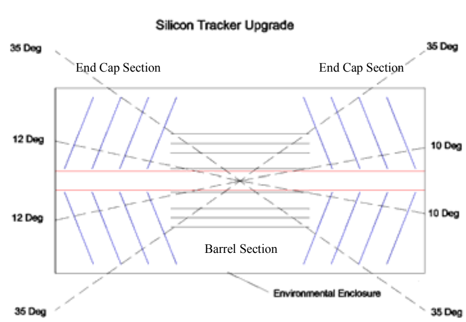

- End Cap Sections:
  - Two Regions, one at each end
  - 4 disk type layers in each Region
  - ALICE type Pixel Detectors
- Barrel Section:
  - 4 barrel type layers
  - Layer 1: ALICE Pixel
  - Layer 2: Either ALICE Pixel or SVX4 SSDs
  - Layers 3 & 4: SVX4 SSDs

Figure 3.1-1: Layout of Detector Layers for PHENIX Tracker.

The end cap regions also have four-disk type layers at each end, which consist of the ALICE pixel detectors. The detector structure is of a clamshell design for installation around the beam pipe. An environmental enclosure exists outside the active regions of the tracker to serve as an enclosure for surrounding the tracker with dry inert gas and to serve as an electromagnetic shield for tracker electronics.

4. Concept Study Structural Analysis

4.1 Material Selection

The selection of materials for the PHENIX detector support structure was based upon several criteria. The most important qualities of the material for the structure are high radiation length, low density, high stiffness, and relative availability.

Figure 4.1-1 shows a table comparing possible material candidates. In the table, material properties were selected based upon the criteria stated above for the structure. From the table, three candidates, GFRP, Beryllium, and Carbon-Carbon (C-C), seem the most qualified to meet the stability and performance requirements listed in section 3.0. Even though beryllium has a longer radiation length, and carbon-carbon has a better stiffness to weight ratio, GFRP has good strength and RL properties and works well in sandwich composites. It should also be noted that C-C materials are generally used for thermal design issues rather than as a structural material.

Because of the large variety of commercial graphite fibers available for GFRP composites, GFRP composites have an added bonus of being easily attainable at a lower cost than beryllium or carbon-carbon. Therefore, the concept structure for the PHENIX detector was developed with GFRP sandwich composites in mind. The next step to the selection process was to select a graphite fiber for the GFRP laminate.

Table 4.1-1: Material Selections for PHENIX Tracker Support Structure.

Material[1]	*Radiation Length (eff.) (cm)*	*Elastic Modulus (GPa)*	*Density (g/cm^3)*	*CTE (ppm/K)*
GFRP[a]	25.0	311.7	1.68	-1.13
Beryllium	35.4	290.0	1.84	11.6
Carbon-Carbon[b]	23.0	496.0	1.7 – 1.85	-1.5
Silicon	9.37	131.0	2.33	2.6
Aluminum	8.89	68.9	2.7	23.6

[a]P75/epoxy, unidirectional properties, ~60% Fiber
[b]Unidirectional properties (P120 fiber equivalent), values listed are representative of the particular fiber used.
[1] Miller, W.O., et. Al., *Superconducting Super Collider Silicon Tracking Subsystem Research and Development*, LA-12029, 1990.

4.1.1 Graphite Fiber Selection

Selection of the appropriate graphite fiber for this application was based mostly upon the overall stiffness of the laminate formed from the fiber. Most graphite fibers have on average the same radiation length and density, so these two criteria set for the overall composite did not factor into the selection of the fiber. Overall, stiffness in sandwich composites comes from the elastic modulus of the face sheet laminate and the shear modulus of the honeycomb core. These properties are generally based upon the type of fiber, the fiber volume fraction in the laminate, the number of plies, and the angle lay-up of the plies.

Table 4.1-2 lists the fibers that on average have an elastic modulus above 500 GPa in the fiber direction for a single ply. Of the fibers listed, all are standard fibers used in industry and are generally available at reasonable cost. However, there is a slight increase in cost associated with the higher modulus fibers like XN-80A.

Table 4.1-2: Fiber Selection Matrix for GFRP Composites.

Material	*E_{11} (GPa)*	*G_{12} (GPa)*	*Tensile strength (GPa)*	*Density (g/cm^3)*
YSH-50A	520	13	3.83	2.12
M55J	539	13	4.02	1.91
XN-50A	517	13	3.86	2.14
YSH-70A	720	13	3.63	2.15
XN-80A	786	22	3.65	2.17

To select a particular fiber, the composite material properties in the FE model of the tracker structure were varied according to a fiber selected, and gravitational static analysis was run to see how much deformation would occur. Assumptions for the model were a mass loading for the entire tracker of 6 times the nominal mass of the structure alone, which is at this time a best guess. In addition, an isotropic 6-ply lay-up was assumed for the face sheets with ply angles set at 0,60,-60|s. Based upon the analysis results, any of the fibers listed in table 4.1-2 would provide adequate stiffness. Fiber selection then defaulted to fiber cost and availability, which of all the fibers, M55J is used in many commercial and industrial composite applications and so it is the most cost efficient and readily available of all the fibers listed in table 4.1-2.

4.2 Structural Analysis

The structural analysis was performed in two parts. The first part consists of using FE models and resulting modal frequencies to look at the dynamic stiffness of tracker concepts. The modal lower limit that was agreed upon for the tracker was 70 Hz on a fully loaded structure. The second part used the same FE models to look at static stiffness with a mass loaded structure. The static stability requirements were defined as less than 100 μm gravity sag for the entire structure with repeatability of better than 25 μm.

4.2.1 Dynamic Analysis

Multiple concepts were conceived for the tracker support structure during the initial brain storming session. Several design decisions were made initially based upon prior experience with similar ultra-stable structures like this one. The decision was made to have the concepts reflect a contiguous shell to keep the structure as stiff as possible. The inside diameter of the structure should be as large as possible within the environment enclosure envelope, again for stiffness reasons. The structure should be the same diameter if possible along the entire length of the tracker and since the structure needs to clam shell around the beam pipe, some work will have to be done with the joining of the two halves to get the structure to act as one piece.

With these design decisions in place, concepts were created and then analyzed by FE model. The results were placed in a matrix for comparison to the other concept results. Variations within the concepts included varying sandwich composite thickness, replacing sandwich composites with thinner solid composite laminates, and adding or removing cutouts in the structure for light-weighting purposes. A couple of the concepts had the structure for the barrel section at a slightly larger diameter than the outer layer of barrel detectors. These two dumbbell concept structures had a smaller bending stiffness than if they were the same diameter as the end cap structure. Figure 4.2-1 shows three of the concepts investigated, and figure 4.2-2 shows the associated first mode shape of the concept that had the highest fundamental frequency.

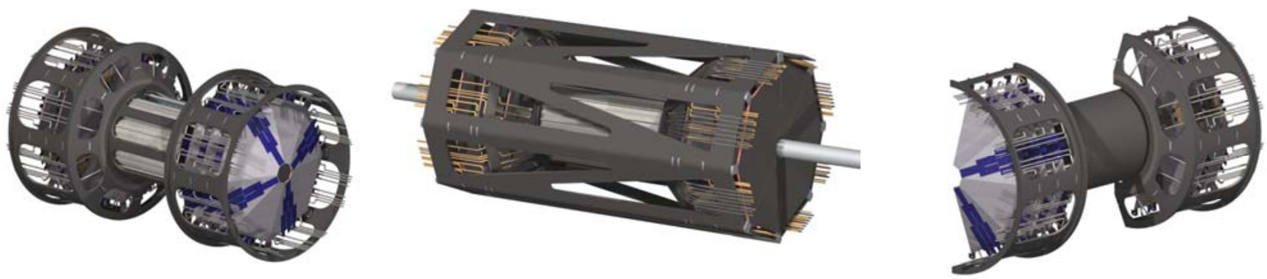

Figure 4.2-1: Various PHENIX Tracker Support Structure Concepts Studied for Structural Stiffness.

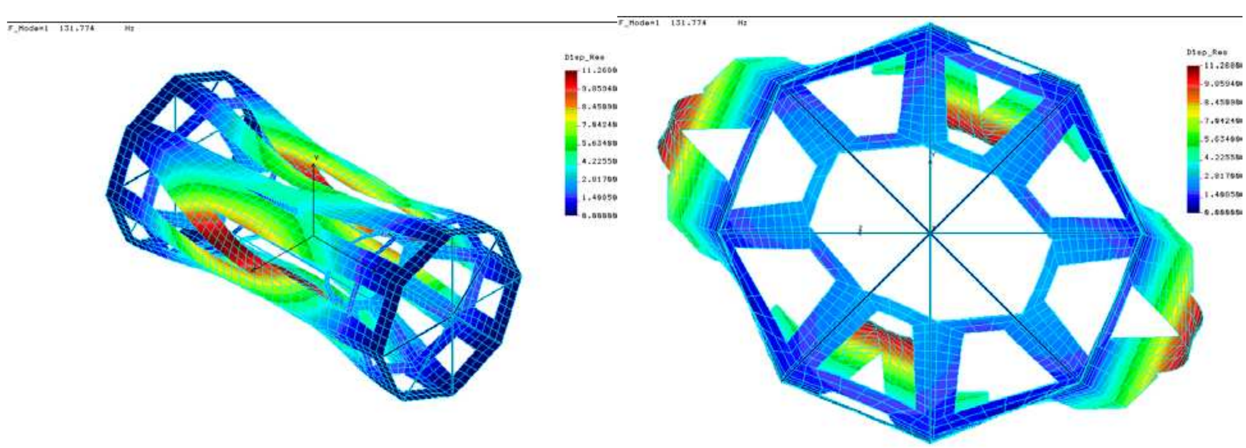

Figure 4.2-2: First Mode Shape (Single Lobe) that Dominated the Dynamic Structural Stiffness Analysis.

Table 4.2-1 lists the first fundamental frequency associated with each of the concepts.

Table 4.2-1: Matrix of PHENIX Tracker Modal Results.

Concept Type	*Mass Loading*	*Mode Shape Type*	*Lowest Fundamental Frequency (Hz)*
Concept #1 No Cross Bracing in Barrel Section, GFRP Composite Sandwich, Dumbbell Config.	Yes	Out-of-Phase Bending	29
Concept #2 Barrel Section Structure is Solid GFRP Shell 0.5 mm thick, Composite Sandwich Const. For End Caps, Dumbbell Config.	Yes	In Phase Bending	32
Concept #3 Entire Support Structure is Solid GFRP Shell, No Sandwich. Light-weighting Cutouts in EndCap Sections only, Dumbbell Config.	Yes	In Phase Bending	53
Concept #4 Entire Support Structure is GFRP Sandwich Composite, No Dumbbell Config., Light-weighting Cutouts in Structure	Yes	Single Lobe	132

Concept #4, shown in figure 4.2-3, with a single large diameter structure has the best overall dynamic stiffness of any of the concepts studied. Concept #4 is unique in that it has a main outer octagonal structure with an inner sub-structure for supporting the barrel detector section and the first two end cap disks on each end. Both the main and inner sub-structures are sandwich composite with cutouts in the panels for light weighting. Large sandwich composite end plates are added for additional structural stiffness.

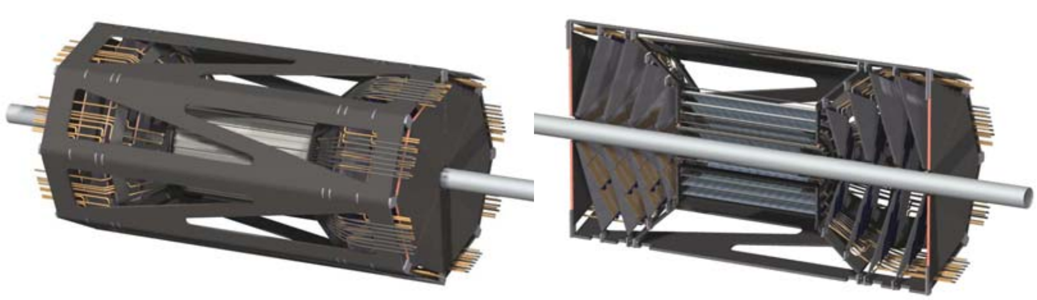

Figure 4.2-3: Concept #4.

From table 4.2-1, the single lobe mode shape became the fundamental mode shape as the barrel region support structure stiffness was increased with concept modifications. In addition, mass and RL became significant with concepts #2 and #3 that used a solid composite shape versus sandwich composite design. This is due to the laminate thickness levels required in the solid composite concepts to get comparative dynamic stiffness.

The end plates for the PHENIX tracker concept #4 were added due to a significant amount of displacement occurring near the support points for the structure due to dynamic loading. Figure 4.2-4 shows the concept #4 FE model without end plates. The additional displacement of the detector support points without the end plates was on the order 3 times as much as with end plates for the single lobe mode shape. The frequency for the single lobe mode shape also dropped to 115 Hz from 132 Hz. The actual first mode shape for the FE model without end plates happens around 58 Hz and is a lateral movement of the detector due to the support restraints modeled. This mode shape disappears with the addition of the end plates. Figure 4.2-5 displays the first mode shape.

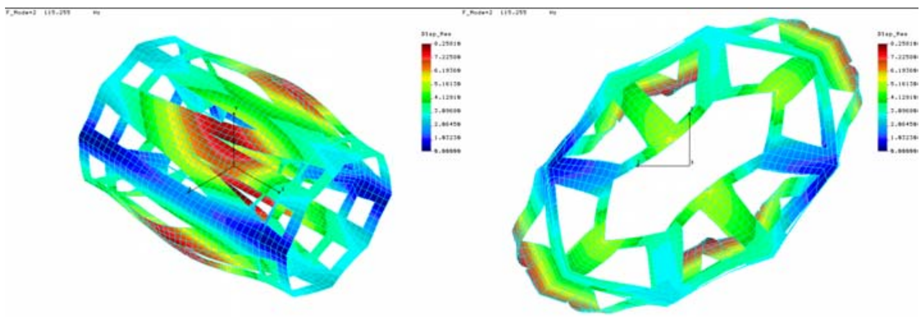

Figure 4.2-4: Additional deformation of Concept #4 without End Plates.

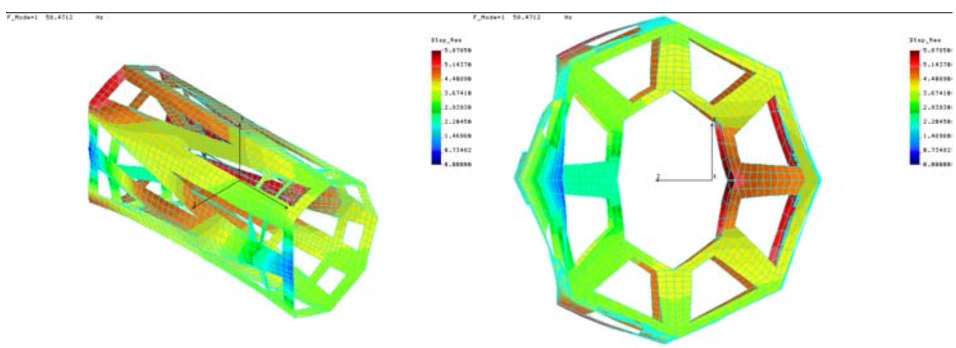

Figure 4.2-5: First Mode Shape for Concept #4 without End Plates.

With a particular concept defined for dynamic excitation, the static analysis was performed on the concept to see how much deflection occurs in the structure and what levels of stress form from the displacement.

4.2.2 Static Analysis

The static analysis was run on concept #4's FE model. A 1.0g gravitational load was applied vertically to the mass loaded structure. Displacements and principal stresses were reviewed against the stability requirement set for the tracker. Figure 4.2-6 shows the resulting displacement and stress.

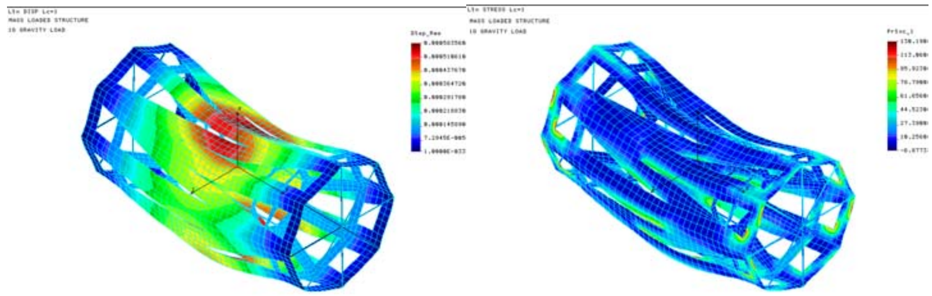

Figure 4.2-6: Resulting Displacement and Principle Stress for 1g Gravity Load.

The maximum displacement on the mass loaded structure was 14.5 μm, and the maximum resulting principal stress was 130 psi.[1] The requirement is 100 μm on the tracker position to account for the initial movement of gravity sag. It is believed that this requirement will be easily met because of the small amount of deformation seen here in the FE model with this concept.

5. Concept Study Cooling Analysis

5.1 Introduction

The coolant system under study is intended for cooling a pixel detector upgrade for the PHENIX Detector (RHIC). The origin of waste heat that must be removed stems from on-board pixel electronics, and their associated power cables. This study covers proposed cooling concepts for the electronic chips in the Barrel region and the pixel electronics in the End Cap region, including a definition of the pixel module local supports. Integration of module cooling and "local" support into a combined structure is defined as a thermostructure for our purposes.

The magnitude and flux density of dissipated electronic heat between the End Cap region and Barrel region for the pixel detector upgrade are both different. The End Cap region is composed of an array of disk-like structures with detectors that have large strip lengths compared to those in the barrel. This increased strip length lowers the heat flux to 0.1W/cm^2 in the End Cap; the contrasting peak heat flux in the barrel pixel layers is 0.7W/cm^2. The combined heat load estimated for the 8-disk layers in the End Cap and the 4-layers in the Barrel region is approximately 2.2kW.

A heat flux of 0.7W/cm^2 is typical of the level under study by the ALICE Pixel Detector (LHC), and at the low end of the heat flux range found in the ATLAS Pixel Detector (LHC). The ATLAS Pixel Detector is physically larger than ALICE and much larger than PHENIX. Developments initiated in ATLAS, more recently applied in ALICE, will be useful in formulating an approach for the PHENIX pixel detector.

[1] Global stress, does not include stress concentration at tracker mount reaction points.

It is worth noting that after much development ATLAS decided on a phase change coolant system, as opposed to a single-phased water-based coolant. Allowing the coolant to change phase makes for a more efficient utilization of the coolant, reducing the total mass flow markedly. This is important for ATLAS, since their total dissipated power in the inner detector volume alone is over 30kW. However, it is our understanding that ALICE is in the process of changing from a single-phase to a two-phase coolant system. The ALICE design is a smaller pixel detector than ATLAS, with much lower dissipated total power (pixels ~2 to 3kW); nonetheless, the higher performance two-phase coolant system has become their primary focus. It is not clear at this stage why ALICE abandoned their first cooling approach.

The two-phase coolant system approach brings with it serious system implementation issues, primarily temperature and pressure control, which we wish to avoid if practical. Consequently, our preliminary coolant study will be based on using the coolant without allowing for phase change. If we find it advisable to convert to a phase change system, we will endeavor to seek a simpler implementation scheme than now under development for LHC. The smaller size, lower total heat load, embodied in the PHENIX pixel detector design may afford us this option.

5.2 Discussion

5.2.1 Coolant Selection

5.2.1.1 Background

In recent years there has been numerous single-phase coolant candidates considered for cooling pixel detectors. Most generally, the concepts evolved around restricting the system design in the detector volume to a laminar flow regime. This choice was judged prudent to avoid potential vibration of the lightweight cooling structures. We are unaware of any real solid evidence that this stringent requirement was necessary. A consequence of this early decision was the emergence of water based-coolants[2] as a natural single-phase choice.

In LHC, the inner detectors see a rather extreme radiation environment; thus, to limit radiation damage the detectors are sub-cooled. To provide their desired detector temperature of -7°C required an inlet temperature of approximately -15°C. As water is quite efficient as a coolant, a blend of water-methanol evolved to satisfy the depressed temperature state. A water-based coolant however, raised a serious concern regarding compatibility with detector electronics. To offset this concern, the system development for a time focused on operating the flow system under a negative pressure. At this point, a more serious issue emerged; a negative system pressure limited the total pressure drop to one atmosphere. This limited pressure head had to be apportioned throughout the detector volume and experimental hall. In the end, a facility decision that placed the refrigerators far from the detector volume made this approach impractical.

A parallel investigation using perfluorocarbon coolants from 3M in a phase change (evaporative) system provided a much-needed alternative to the impasse that arose. In the current ATLAS-LHC approach, high-pressure (2 atm. and above) coolant is throttled before entering the thermostructure, onto which the detector modules are mounted. The entering fluid ranges in temperature from -15°C to -20°C, which then evaporates while passing through the

[2] Heat transfer in laminar flow is by conduction; hence, fluid thermal conductivity is important. Water thermal conductivity is much higher than other fluid options.

thermostructure. ATLAS barrel pixel modules dissipate 80W, and the use of the latent heat of evaporation to absorb the heat reduced the required mass flow significantly. Adopting the two-phase flow regime, however, brought attendant flow control design issues that had to be addressed. At one point, serious consideration was being given to use of perfluorocarbon candidates as a single-phase coolant, taking the increased radiation length penalty as a necessary consequence for a simpler approach.

It is worth noting that the two-phase flow is associated with substantial flow turbulence, however, this condition did not result in instabilities in the lightweight structures. This fact further substantiates our belief that turbulent flow in a single-phase system for this application is acceptable.

For PHENIX, we plan to adopt a single-phase coolant approach, using one of the perfluocarbon candidates. We benefit from several obvious differences from ALICE and ATLAS, namely:

- Far lower total waste heat that must be removed, 2.2kW versus 3 to 15kW for LHC detectors
- Much lower localized heat flux, $0.1W/cm^2$ for the disks, and a tolerable level of $0.7W/cm^2$ for pixel barrel ladders

In addition, we propose to use a turbulent flow regime for improved heat transfer, thus overcoming the low specific heat and low liquid thermal conductivity inherent in these fluids.

5.2.1.2 Coolant Candidates

Table 5.2-1 comprises a list of perfluorocarbons produced by 3M, commonly referred to as "fluorinerts". These carbon-fluorine based fluids replace standard halogen refrigerants that proved to be environmentally unacceptable. These fluids can be used as either a single-phase or a two-phase fluid. One will note that the latent heat of vaporization provides a significant performance advantage over the specific heat capacity that governs the sensible heat pickup in a liquid substance, providing impetus to using two-phase flow in high heat load applications.

Table 5.2-1: Selected Perfluorocarbon Fluid Properties @ 1 ATM.

Coolant	Saturation Temperature (°C)	Specific Heat (kJ/kg-°K)	Density (kg/m^3)	Latent Heat of Vaporization (kJ/kg)	Thermal Conductivity (W/mK)	Viscosity (µPa-s)
C_5F_{12}	29.75	1.090	1597.2	91.89	0.0425	305.04
C_4F_{10}	-2.09	1.029	1591.3	96.96	0.0470	305.25
C_3F_8	-36.6	0.968	1604.1	104.78	0.0651	313.8
C_6F_{14}	56	1.088	1680.0	87.9	0.0545	450
CH_3OH	64.4	2.825	748.4	1101.2	0.306	503.6

A fundamental parameter that one should consider in detector cooling is the fluid saturation temperature, i.e. simple boiling. One atmosphere is chosen for a customary reference when comparing fluids. For example, C_5F_{12} would boil at 29.75°C, hence this fluid is suitable for single phase cooling below this point at 1-atm, or above, assuming an increased operational pressure is chosen. A system pressure higher than 1-atm, coupled with a sub-cooled liquid state will insure no boiling occurs. We look for a fluid candidate that does not require a high pressure to suppress boiling, but sufficient as to provide for adequate pressure drop in the flow circuit. For this reason, one would not choose to use C_4F_{10} or C_3F_8 for PHENIX, unless detector sub-cooling becomes of interest. To permit operation with these fluids at near room temperature would require a high-pressure system, by at least HEP detector standards. For the ATLAS Pixel Detector, both fluids were chosen for two-phase coolants candidates, with C_3F_8 chosen as the most suited to provide a base-inlet temperature of -15ºC.

Included in this table is methanol, a fluid frequently used in heat pipe applications because of its high latent heat of vaporization. This fluid also has a high specific heat capacity making it appropriate for single-phase cooling. Although its density is lower than the other candidates, the product of density with specific heat capacity is still higher.

In figure 5.2-1 the saturation curve for C_5F_{12} and C_6F_{14} are depicted for a range in temperature. We choose as a preliminary design point[3] for PHENIX cooling inlet 20ºC. Based on this figure we must maintain a system return pressure above 9psia and 4psia for the two fluids respectively, otherwise boiling will occur. Boiling in the return circuit will be deleterious to maintaining a reliable pump inlet suction pressure.

If the pump discharge pressure is set for example at 30psia (~15psi differential), the maximum pressure loss that can be accepted in the overall flow circuit is 16psi and 21psi for C_5F_{12} and C_6F_{14} respectively. This would provide a 5psi margin (either case) with respect to boiling. Higher discharge pressure can be considered, as long as the thermostructure is designed to resist this pressure with minimum distortion.

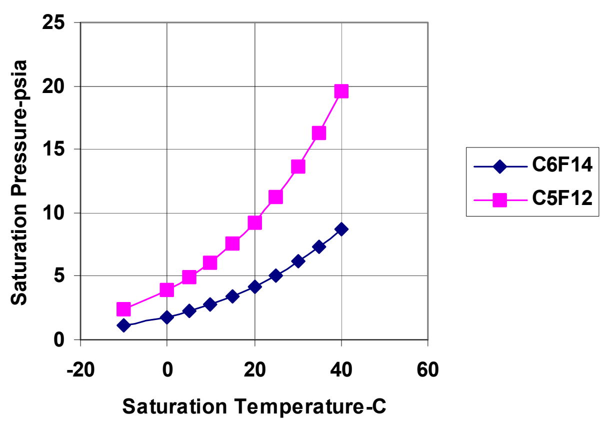

Figure 5.2-1: Saturation pressure displayed versus saturation temperature for two potential liquid-based cooling candidates.

In selecting the average operational temperature of 20ºC, it is understood that the incoming temperature will be lower and the exit temperature higher, i.e., a small bulk fluid ΔT effect. This ΔT can be managed by adjusting the quantity of heat pickup (several thermostructures in series), or mass flow rate, for a given fluid specific heat capacity. In making

[3] A request was made to consider a cooling range of 0 to 20°C. For the initial study we will use the value indicated; sub-cooling will be provided if judged necessary.

these parameter adjustments, it is in general desirable that we limit this ΔT, as well as the temperature gradient in the module support structure.

5.2.2 End Cap Discussion

The PHENIX Pixel Detector forward regions as presently envisioned consist of a conical array of modules, with 4-such arrays at each end. Dissipated heat from the modules is assumed evenly distributed at 0.1W/cm^2. Conceptually, we have chosen a flat octagonal panel structure, with modules mounted on alternating panels, i.e., front to back. Figure 5.2-2 depicts this arrangement; each flat panel is denoted as a *disk sector,* for purposes of discussion. In the largest disk sector, the total heat is approximately 15W, or a total of 120W for a complete clamshell disk.

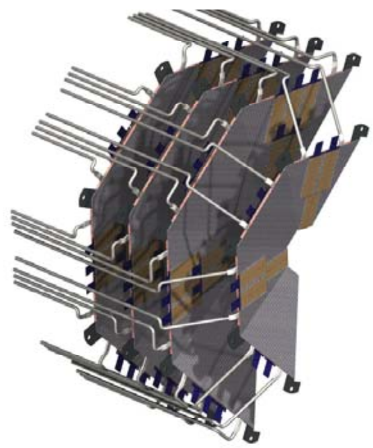

Figure 5.2-2: 3D model of octagonal disk-like structures for supporting the PHENIX Pixel modules in the End Cap region. One-half of each octagonal disk is illustrated; the individual structures clamshell around the beam pipe on the vertical plane.

An on-going task of the cooling study will be to optimize this overall structure, and the disk-sector substructure that contains an embedded cooling channel or tube for removing heat from the module electronics. As figure 5.2-2 suggests, we plan a continuous structure for each *half* of the clamshell. In PHENIX, two considerations came into play in choosing this arrangement. First, the radial extent of the disk-sectors is rather large, and secondly, the structure must be clam-shelled. Mounting the disk-sectors individually onto a composite ring, as we did for ATLAS, very likely would present a structural stability problem for PHENIX. The reason for individual sectors in ATLAS was to facilitate assembly and alignment of the modules, and ease of handling of small components. In ATLAS, modules are mounted on both sides of an individual sector, whereas in PHENIX modules are mounted one side of the "local" support structure. This asymmetry introduces the potential for out-of-plane distortions in the PHENIX sector.

5.2.2.1 End Cap Cooling Tube Sizing

Figure 5.2-3 depicts a cross-section schematic of two possible sandwich structures with an embedded cooling tube. The primary difference between the two illustrations is the configuration of the cooling tube, in one case circular, and the other elliptical[4]. In general, elliptical or flat walled tubes provide better contact with flat sandwich facings, but this squashed tube profile does result in an overall thinner sandwich structure, and less stiffness. The circular tube because of its limited contact with flat surfaces needs some form of contact enhancement to reduce the thermal contact resistance. This may take several forms, but the simplest is to add material around the tube.

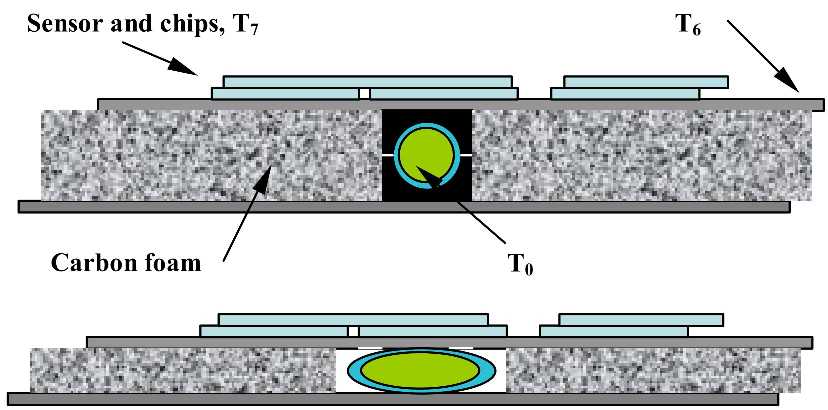

Figure 5.2-3: Illustration of embedded cooling passage arrangement in a composite sandwich. Upper inset depicts a circular tube and the lower inset a flatten tube, which enhances heat transfer at the expense of sandwich thickness.

The temperature gradient from the pixel module surface to the bulk coolant is set by the thermal resistances of numerous contributors, namely:

- ΔT_{0-1}: Coolant film temperature drop at the tube containment wall
- ΔT_{1-2}: Temperature drop through tube wall material
- ΔT_{2-3}: Temperature drop through adhesive, or thermal grease surrounding tube
- ΔT_{3-4}: Temperature drop of tube interfacing material
- ΔT_{4-5}: Temperature drop through sandwich facing to tube interfacing material
- ΔT_{5-6}: Temperature gradient in sandwich facing from the electronic chip to the cooling tube location
- ΔT_{6-7}: Temperature drop in the adhesive used to mount the module chip to the sandwich facing

One may note that two thermal resistances are unique to the tube physical size, i.e., resistances ΔT_{2-3} and ΔT_{3-4}. Resistance ΔT_{3-4} can be minimized by using a highly conductive carbon-carbon material. It is advisable to limit the number of adhesive interfaces, i.e., resistance ΔT_{2-3}, because the material as a class is a rather poor conductor of heat. The heat flux and temperature gradient

[4] Extruded rectangular tubing is also an option.

increases as the area for conduction decreases; one potential area occurs at the tube wall, where the thickness of an adhesive must be controlled carefully.

Figure 5.2-4 depicts the bulk fluid temperature rise that must be considered in an estimate of the module maximum temperature. Modules near the coolant outlet will be at a higher temperature than modules near the inlet by the amount shown. In addition, if we choose to connect the disk sectors in series the temperature will increase by this amount. For the range of mass flow chosen, the added temperature term can be limited to 1.5ºC.

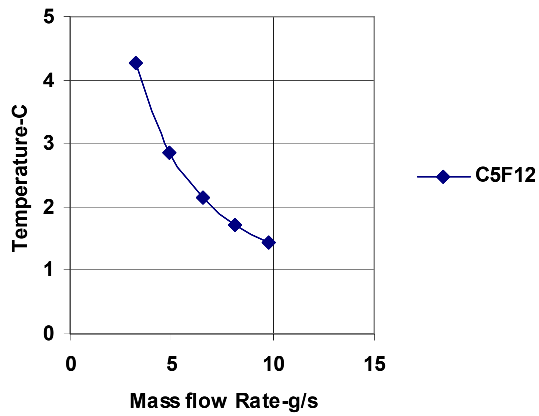

Figure 5.2-4: Bulk fluid temperature rise versus mass flow rate for C_5F_{12} perfluorocarbon (3M). Single-pass through a full size End Cap disk sector; heat dissipation of 15W.

We have chosen a tube path length of 550mm in the large disk-sector as a departure point in sizing the cooling passage for the End Cap region. For a selected range in mass flow rates, pressure drop was calculated for chosen tube diameters, figure 5.2-5. The indicated pressure drop allows for a number of 180º bends to cover the meandering tube path, which is necessary to cover the sector area fully. With a 2mm inner tube diameter and the maximum flow rate, the estimated pressure drop would be nominally 6psi. The pressure drop in an equivalent elliptical tube would be higher, which we can reduce by increasing the tube hydraulic diameter. In addition, if we chose a series connection of two sectors; two sectors result in a 12psi drop, which appears acceptable.

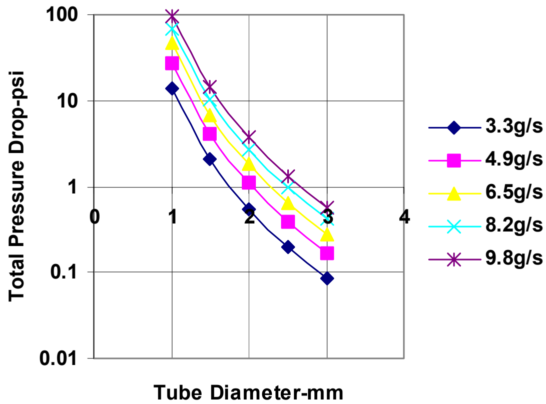

Figure 5.2-5: Pressure drop for turbulent flow in a single-pass through a full size End Cap disk sector, shown as a function of inner tube diameter and mass flow for C_5F_{12} fluid at 20°C. Tube length, L= 550mm.

The estimated pressure drop must be increased by losses in the inlet and return passages. However, at this point it looks like we are within our constraints to avoid boiling in the return line. This additional pressure loss contribution can be added once the distance from the detector to the cooling system chillers is known.

By using turbulent flow, the temperature gradient in the coolant film is minimized. Figure 5.2-6 illustrates an essentially linear dependence of ΔT_{0-1} with tube diameter, for a constant mass flow. As tube diameter increases, surface area for heat transfer increases, so one would expect the film temperature drop to decrease. However, the fluid heat transfer coefficient is a strong function of Reynolds number, which is decreasing with increasing surface area. One sees for a given tube diameter this effect can be offset by increasing the mass flow. For example, ΔT_{0-1} is the same for a 1mm diameter tube as for a 3mm diameter tube when the flow is increased from 3.3 to 9.8g/s. However, one should not jump to conclusion that a 1mm diameter tube is an appropriate choice until the temperature gradient in the adjacent interfaces is determined.

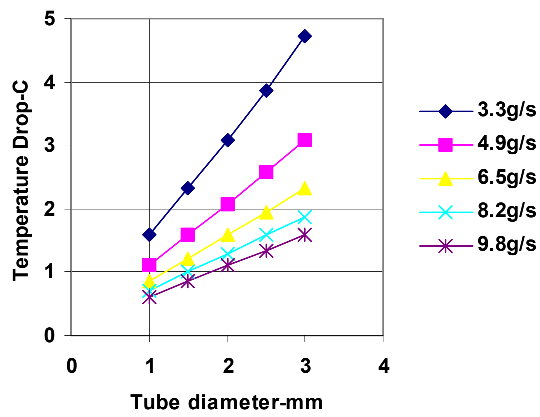

Figure 5.2-6: Temperature gradient in the coolant film, $\Delta T_{0\text{-}1}$, as a function of inner tube diameter for various C_5F_{12} mass flow rates. Based on 15W dissipated in a full size End Cap disk sector.

5.2.2.2 Sector Radiation Length Estimate

A first order approximation is made for the radiation length in the thermostructure as a function of tube inner diameter. Figure 5.2-7 depicts the individual and combined radiation length for the materials comprising the sandwich. The thickness terms used in the calculation are:

- Al tube, 200μm (0.008 inch wall)
- 4mm carbon foam separator, 5% mass density
- tube support 2mm wider than tube diameter
- sandwich facings, 400μm

We estimate for this thermostructure roughly 0.5 to 0.6% for a tube diameter in the range of 2mm to 3mm in inner diameter, including coolant, figure 5.2-7. The PHENIX design goal is 0.5% for the cooling and support structure.

The radiation length may be decreased through further design study with an elliptical or extruded rectangular tube. However, we need to make a more elaborate model that brings in structural mechanics considerations. A first order approximation of these structural aspects is discussed in the next section.

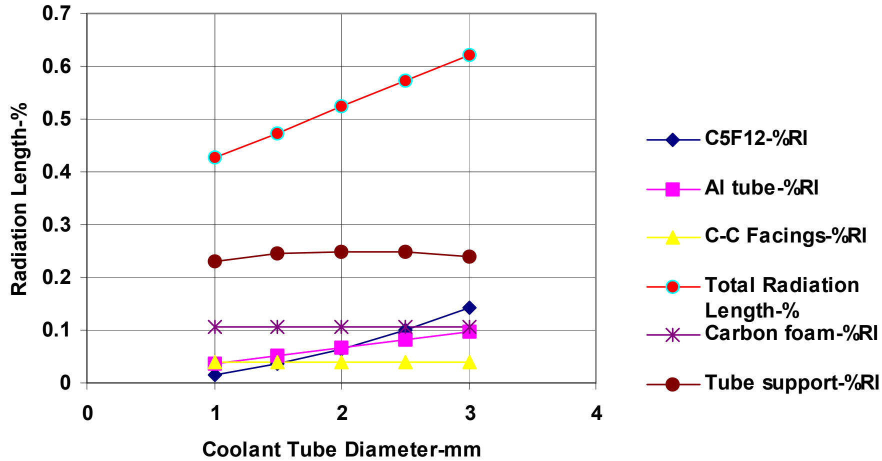

Figure 5.2-7: Estimated normal radiation length for End Cap disk sector for various tube inner diameters, and for a fixed separation between sandwich facings of 4mm. Coolant designation is C5F12.

5.2.2.3 Sector Thermal Considerations

Table 5.2-2 summarizes an estimate of the temperature differential for each of the thermal resistances cited earlier for four coolant tube diameters (ID). For the assumed conditions there are three dominant contributors, namely, the tube support ($\Delta T_{2\text{-}3}$), adhesive bond between tube support and sector facing ($\Delta T_{4\text{--}5}$), and in the sector facing ($\Delta T_{5\text{-}6}$) onto which the modules are mounted. The listing does not include the temperature drop of the adhesive joining the module to the facing.

This list is at best a rather crude estimate for a round circular tube mounted in a sandwich, but it is not probably far off. One will note that the two largest contributors are fluid film temperature gradient and the thermal gradient in the composite facing, which is essentially independent of the tube geometry, but strongly dependent on tube spacing. Tube spacing was set at 2cm, as will be explained later.

Table 5.2-2: Estimated Temperature Gradient for End Cap Disk Sector with 9.8g/s of C_5F_{12}.

Tube ID (mm)	$\Delta T_{0\text{-}1}$ (°C)	$\Delta T_{1\text{-}2}$ (°C)	$\Delta T_{2\text{-}3}$ (°C)	$\Delta T_{3\text{-}4}$ (°C)	$\Delta T_{4\text{-}5}$ (°C)	$\Delta T_{5\text{-}6}$ (°C)	Sum (°C)
1.0	3.81	0.016	0.93	0.033	0.46	2.27	7.52
2.0	1.97	0.008	0.51	0.023	0.46	2.27	5.24
2.5	1.61	0.007	0.42	0.02	0.46	2.27	4.79
3.0	1.36	0.006	0.36	0.017	0.46	2.27	4.47

We chose for the first approximation, based on prior experience, a facing constructed from carbon-carbon (C-C) material with a thermal conductivity of 200W/mK and a thickness of 0.44mm. C-C material has a very high, through the thickness, thermal conductivity, which reduces the thermal gradient from the pixel module into the facing material. With more time, we will look into a resin-based composite facing option, if directed. However, we realize that in doing so we must undertake a more thorough analysis, and most likely thermal testing.

A necessary consideration in determining this gradient is the distance which heat must flow transversely to the nearest tube. Letting the separation between tubes be L, then this temperature gradient, which is caused by a uniformly distributed heat source, varies as the distance L^2. The shortest possible distance consistent with acceptable radiation length is desirable. Experience has shown this distance to be about 2cm. To control and to minimize the distance from any module on the sector face we resort to a meandering tube path, figure 5.2-8.

We must add to the temperature list in table 5.2-2 the rise in bulk fluid temperature, to obtain the peak module temperature. For the 9.8g/s the bulk fluid would increase by 1.43°C, bringing the estimated peak module temperature to 6.67°C above the inlet temperature. If the coolant were supplied at an inlet of 20°C, the peak temperature in the sector would be roughly 26.7°C.

Series connection of two adjacent sectors is plausible, since the bulk fluid temperature rise per sector is low. This design aspect will be evaluated in the final design analysis.

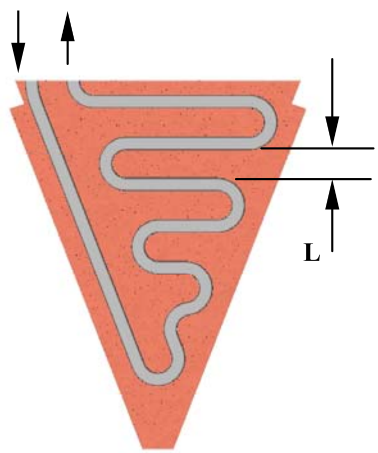

Figure 5.2-8: First order coolant path geometry selected for the largest disk-like sector in the End Cap region.

5.2.2.4 <u>End Cap Internal Structure</u>

As shown in figure 5.2-2 the disk-like structures are split to allow for a clamshell installation operation. This condition leaves an unsupported edge for two of the sectors that make-up the flat panel sandwich structure. Thermal strains induced by the module electronics are expected to cause bowing of the sectors, with the most pronounced effect being along this parting line. The second potential instability that may be encountered in this region will be due to excitation from vibration. Our objective is to estimate these effects and guide a preliminary selection of the parameters necessary to define the sandwich composite.

5.2.2.4.1 <u>Modal Analysis of the Largest End Cap Internal Structure</u>

A simplified model of the largest half-disk internal structure was formulated. Quadrilateral sandwich elements were used to provide a simulation of the proposed sandwich thermostructure, reference figure 5.2-9. A high modulus, thermally conductive C-C composite is assumed for the facing, with low-density carbon foam for the core. The model facing density was increased to simulate added mass terms for the modules, coolant tube, and coolant. For the sandwich simulation, we chose a 0.44mm facing thickness (a thermal reason, not structural), in conjunction with a 2mm[5] thick carbon foam core. Outer corner restraints fixed movement in all 3-translational degrees of freedom. This degree of rigidity may not be realized through a simple connection of the corners to the outer frame. Nonetheless, the first mode was determined to be 370Hz, much higher than required for dynamic stability.

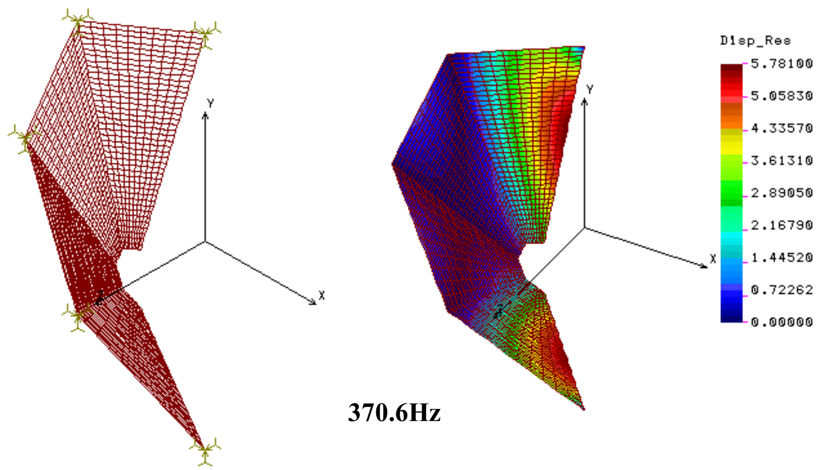

Figure 5.2-9: FEA of a disk-like half structure for mounting the End Cap pixel modules. The structure is supported at each outer corner of the flat-panels that make-up the composite sandwich structure.

5.2.2.4.2 Static Load Analysis of the Largest End Cap Internal Structure

To gain a sense of the static stiffness of the sandwich structure, we chose to impose a simple axial force in the Z-direction (along beam-line). For the first solution, figure 5.2-10, a 1N force was applied at the 4-interior points of the trapezoidal shape disk sectors. This force, equivalent to 0.25lbf (4 oz), resulted in a 5.3µm motion at the point of load application. A second 1N arbitrary load was applied at midway along the unsupported edge. In this instance, the response was somewhat greater, 19.9µm, as one may expect. It seems clear that from this simplified analysis that the static stiffness of the sandwich, particularly the unsupported sector edge, is of greater concern than the dynamic stiffness. At this juncture it does not seem prudent to reduce the sector facing thickness of 0.44mm, which we originally chose from thermal considerations, in spite of one might like to do from a radiation length consideration.

[5] This sandwich is thinner than assumed for the coolant analysis. Assuming the structural stiffness proves adequate, we will want to revise the method of joining the cooling tube to the C-C facing.

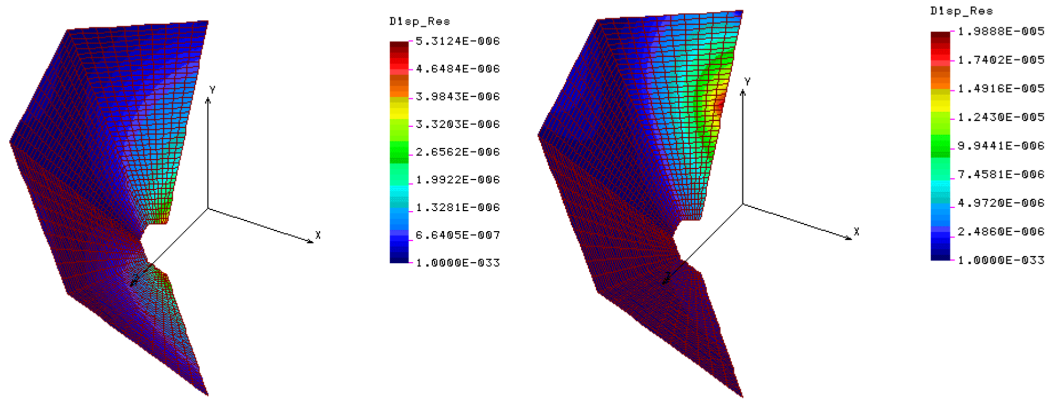

Figure 5.2-10: Static solution of End Cap half disk-like, structure. Load condition for model in left inset is 1N (0.25lbf) axial, distributed at the 4-inner corner points, which results in a 5.3μm axial movement. Load for model in the right inset is 1N in axial Z-direction on the outer unsupported edge, resulting in a 19.9μm distortion.

5.2.2.4.3 Thermal Solution for the Largest End Cap Internal Structure

Thermal distortion of the half-disk sector along the unsupported edge is a distinct possibility, since numerous construction materials with different coefficients of thermal expansion are involved. A first order cooling approximation indicates that the temperature gradient should be less than 10°C, which mitigates this issue. PHENIX design requirements state that the structure may possibly be cooled down to 0°C, and this may lead to increased distortion. To properly assess this effect, a thorough 3D FEA of the End Cap half-disk structure is recommended for qualifying the final design. For purposes here, we will attempt to quantify the magnitude of the distortion with our composite shell model.

The previous composite laminate shell model is used to predict the distortions in the basic structure; however, coupling from the pixel modules to laminate facing are not included. Although, module mounting will be accomplished with a compliant adhesive, we know from experience that the difference in CTE between these two materials, module and laminate, will contribute further to the local distortion.

Figure 5.2-11 illustrates the estimated distortion from applying a 10°C temperature gradient through the sandwich structure, without the pixel modules included. The magnitude of distortion is small, due to the small gradient, and the stiff sandwich structure. It is difficult to assess how realistic is this simulation because of the complexity of the problem. Until a complete 3D model is constructed, we must assume that the distortion along the unsupported edge will be less than a few microns.

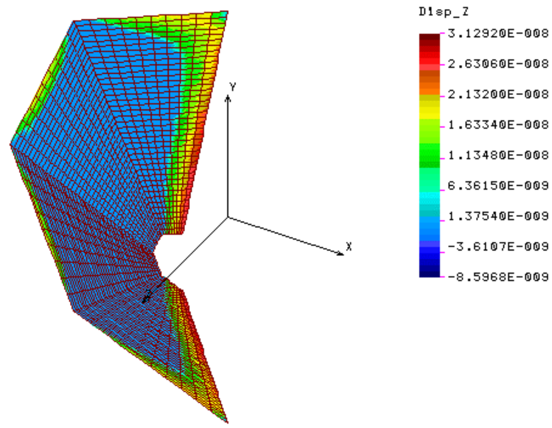

Figure 5.2-11: Static solution of the clamshell sandwich model with a 10°C temperature differential normal to the sandwich facings. Localized distortion along the unsupported edge is 0.031μm.

5.2.2.5 End Cap Analysis Summary

First order calculations were made for the largest internal structure proposed for the End Cap. Based on these preliminary analyses it is concluded:

- Single-phase perfoluorocarbon fluid, e.g., C_5F_{12}, is well suited to cooling, without a phase option being necessary.
- Assuming a 0.1W/m^2 evenly distributed heat flux from the pixel modules in the End Cap region, it appears reasonable to connect two adjacent disk-sectors in series, reducing the number of service connections by half.
- To minimize pressure drop and to permit series connections of two adjacent sectors, it is recommended that a 2mm to 2.5mm ID tube be used
- To facilitate heat transfer from the sector facing to the coolant, it is recommended that an elliptical (squashed tube) or extruded rectangular tubing be used
- Sandwich core thickness of 2mm appears adequate for attaining desired stiffness
- The bare sandwich disk-like clamshell structure, no modules included, should have a radiation length on the order of 0.6%.

5.2.3 Barrel Region Discussion

5.2.3.1 Barrel Description

Our preliminary design concept for the barrel region draws on a stave (*or ladder*[6]) concept for supporting both the inner two layers of pixels and the outer two strip detector layers. The pixel detectors and strip detector array are arranged in a longitudinal fashion, and at a slight cant angle, which provides a small amount of overlap for hermeticity. The pixels and silicon

[6] Ladder will be used interchangeably with stave connotation

strip detector both contain on-board electronics, thus necessitating cooling along the Z-axis of the detectors.

Since the barrel region is short, 30cm in length, it is presumed that the staves need only be supported at their ends[7]. Open ring like structures at the two ends of the staves, figure 5.2-12, provide attachment points for the staves and serve to combine the staves into two halves of a clamshell. Figure 5.2-12 also illustrates the cross section of a stave-like structure. This structure is composed of a thermal plane onto which the pixel modules or strip detectors are mounted. The thermal plane collects the distributed electronic heat, as well as providing a conductive path to the cooling tube. We choose a highly conductive, high modulus 2D C-C material for this thermal plane. To make an efficient joint of the coolant tube to the thermal plane, we choose a 3D C-C material. All three elements are bonded with thermally conductive, rigid setting adhesives.

A significant portion of the stave stiffness is provided by the OMEGA piece, which is bonded to the thermal plane. The OMEGA piece is important when handling a fully assembled, module-populated unit.

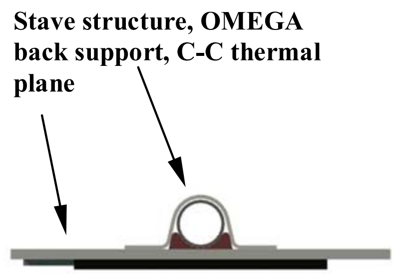

Figure 5.2-12: 3D CAD model of barrel region clamshell and a typical stave geometry chosen for preliminary thermal and cooling analysis.

There are several concerns with this approach:

- Out-of-plane distortions from thermally induced strain, caused by differing CTE's
- Gravity sag of the upper and lower stave elements, resulting in deflections of greater than allowed by assembly requirements
- Mass of the structure exceeding the radiation length guidelines

To gain an appreciation of these issues we chose as a starting point sizing a ladder for one of the silicon strip layers. This ladder has the greatest total heat load, 27W, which affects the cooling tube sizing. However, it actually has a lower dissipated heat flux, which reduces the component peak temperature, mitigating the thermal strains to some extent.

[7] This point is an essential ingredient of this design and must be explored and proven.

5.2.3.2 Temperature Gradient Estimations

Following the same form chosen for the End Cap region, we made an estimate of the various temperature drops in the stave assembly:

- ΔT_{0-1}: Coolant film temperature drop at the tube inner wall surface
- ΔT_{1-2}: Temperature drop through tube wall material
- ΔT_{2-3}: Temperature drop through a compliant adhesive, or rigid adhesive joining the tube to tube support
- ΔT_{3-4}: Temperature drop of tube interfacing material
- ΔT_{4-5}: Temperature drop in a rigid adhesive joining sandwich facing to tube interfacing material
- ΔT_{5-6}: Temperature gradient in sandwich facing from the edge of the strip detector to the cooling tube location

As before, the analysis proceeds with hydraulic calculations of pressure drop for various flow rates, which provides some visibility on tube size limits. Bulk fluid temperature rise is independent of tube size and pressure drop; this parameter ranges from a high of 1.93°C to a low of 1.1°C for a mass flow range of 13.1 to 22.8g/s, corresponding to a heat pickup of 27W, figure 5.2-13. A noticeable rise in fluid temperature will occur for mass flow rates below 13g/s, which we wish to avoid.

Figure 5.2-13 also depicts the frictional loss for the fluid flowing under turbulent conditions.[3] For the moment we set as an objective to keep bulk fluid temperature rise to less than 2°C and frictional pressure drop to less than 2psi. These assumptions will easily permit series connection of two staves, and possibly more if one chooses. This decision will be revisited later.

From Figure 5.2-13, pressure drop for a 1mm inner tube is very high for all indicated mass flow rates. To lower this parameter to within acceptable bonds would require a substantial reduction in mass flow rate and a corresponding undesirable increase in bulk fluid temperature rise. We see that our stated objectives are best satisfied with a tube diameter of 2.5mm, or larger.

To proceed with the next step, i.e., examining the structural implications of the stave, we chose a 3mm inner tube diameter. By making the coolant tube part of the structure, the out-of-plane stiffness will be enhanced. This decision favors a large diameter tube. If small diameter tube were used it will contribute mostly mass and little stiffness, the benefit being lower radiation length.

In table 5.2-3, we list the estimated peak temperature differential and contributors. We note that there are three pronounced contributors: coolant film[3], adhesive film between tube and tube support, and the C-C thermal plane. However, the overall temperature differential appears to vary little with tube diameter. At a small tube diameter, the heat flux through the adhesive, which is a rather poor conductor, is high. This increase in temperature gradient is largely offset by the improved fluid heat transfer in the more turbulent, higher velocity fluid.

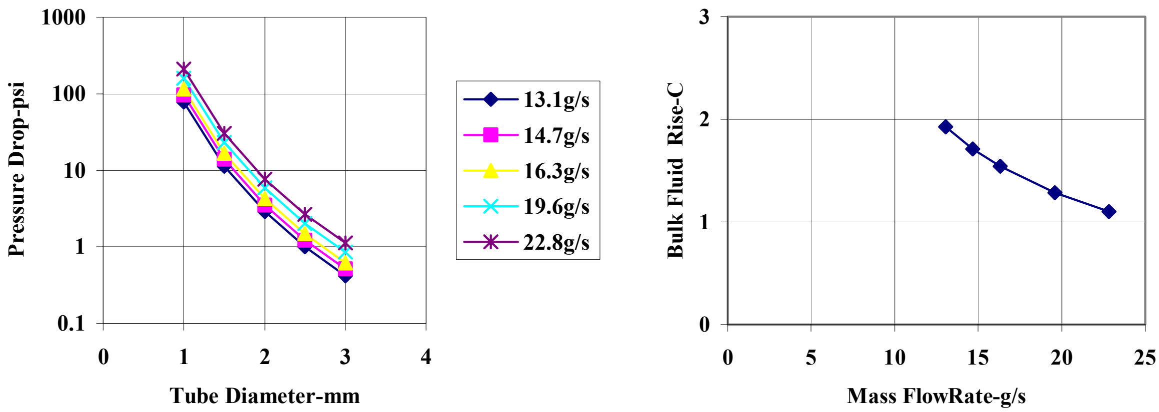

Figure 5.2-13: Right inset illustrates coolant bulk temperature rise versus mass flow rate, for 27W heat load. The left inset depicts tube pressure drop as a function of the coolant mass flow rate. Pressure drop is for a single 30cm long stave only, estimation of fittings and elbows are not included.

Table 5.2-3: Listing of Temperature Drops through Various Elements Comprising a Stave for 22.8g/s.

Tube ID (mm)	ΔT_{0-1} (°C)	ΔT_{1-2} (°C)	ΔT_{2-3} (°C)	ΔT_{3-4} (°C)	ΔT_{4-5} (°C)	ΔT_{5-6} (°C)	Sum (°C)
1.0	1.2	0.026	2.87	0.94	0.75	2.9	8.69
2.0	2.1	0.014	1.59	0.75	0.75	2.9	8.10
2.5	2.6	0.011	1.30	0.68	0.75	2.9	8.24
3.0	3.05	0.009	1.10	0.62	0.75	2.9	8.40

To advance the design we elect to use a 3mm diameter Aluminum tube with a 0.2mm wall thickness. Both, the thermal plane used for module support and the tube support, are based on C-C materials. The OMEGA piece is a compression molded resin based composite.

5.2.3.3 Stave Thermal Solution

As a first step, we analyze the temperature distribution through the stave cross section using a FE model. Adhesive layers in practice tend to be on the order of 75µm, which are difficult to represent in an FEA. We chose to adjust (decrease) the thermal conductivity of the structural materials to account for this omission.

The first FE model is a simple planar one, illustrated in figure 5.2-14. A heat flux of 0.35W/cm^2 is applied to the silicon surface and a convective film coefficient of 3000W/m^2 is applied to the inner tube surface. COSMOSM is used to solve for the thermal distribution. The coolant film coefficient was obtained from the earlier tube sizing effort.[3]

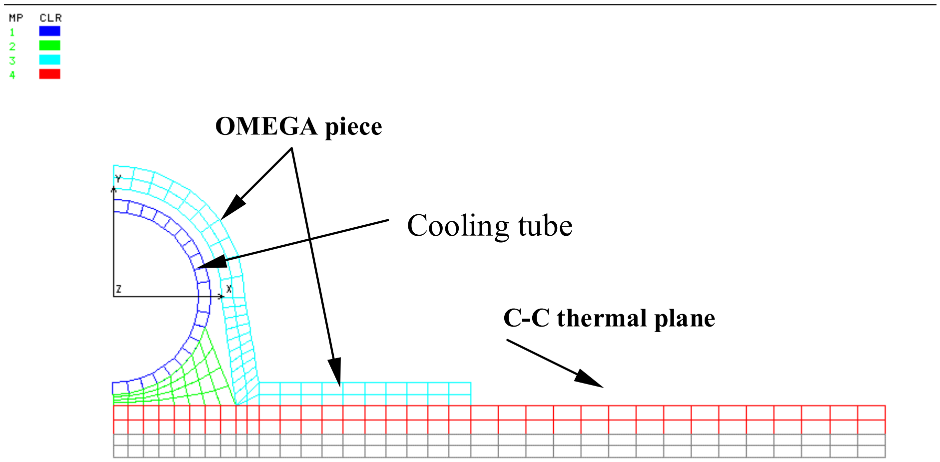

Figure 5.2-14: FE stave model representing support for silicon strip detector, typical of layer 3 and 4. FE model represents the composite structure only, with a C-C thermal facing thickness of 0.5mm and an OMEGA wall thickness of 0.4mm. The cooling tube is 3mm ID with a 0.2mm wall thickness. The solution is for uniform heat flux of 0.35W/cm^2 and a coolant temperature of 20°C.

Figure 5.2-15 depicts the thermal gradient through the structure shown in figure 5.2-14. We note several facts. One, the temperature gradient in the coolant film ranges from 2.67°C to 4.0°C. The earlier analytic solution, assuming uniform distribution, was 3.05°C. Secondly, temperature difference between the outermost module point and close to the junction of the tube support with the C-C facing is nominally 1.4°C, whereas the earlier estimate was 2.9°C. Third, the overall FEA gradient is 6.13°C, and previous estimate 8.4°C, a difference of 2.3°C. There are several explanations for these differences.

First, the FE model illustrates that the heat picked up by the coolant is not uniform around the tube circumference, which the analytic solution assumed. We see that the analytic solution is bounded by the FEA distribution, which we expect.

Secondly, the FEA included the heat conducted by the silicon module and the 1st order analytic expression did not. Heat conducted by the silicon dropped the peak temperature by approximately 1.5°C. In the final ladder design, when is more is known about the module construction, this point should be revisited. In addition, we may need to revise the silicon module thickness used in the FEA.

In so far as the overall peak gradient differing by 2.3°C, it is felt most of this is due to some of the heat being conducted by the silicon. This point will be made more conclusively in a more refined study.

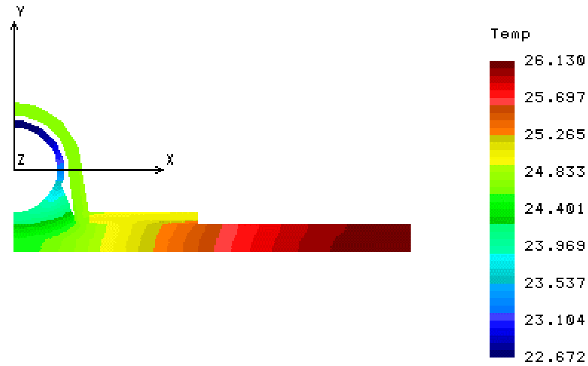

Figure 5.2-15: Thermal solution with 0.4mm thick silicon layer. Heat flux, 0.35W/cm^2, applied to surface of silicon. Continuous layer of silicon contributes to the conduction of heat to the coolant tube.

Figure 5.2-16 illustrates the out-of-plane distortion in the stave for the temperature distribution of figure 5.2-15. The reference temperature used for a strain free condition was 25°C. Since the temperature rise in the structure does not depart from this condition significantly, the distortion of the edges is quite acceptable, a peak of 0.18μm.

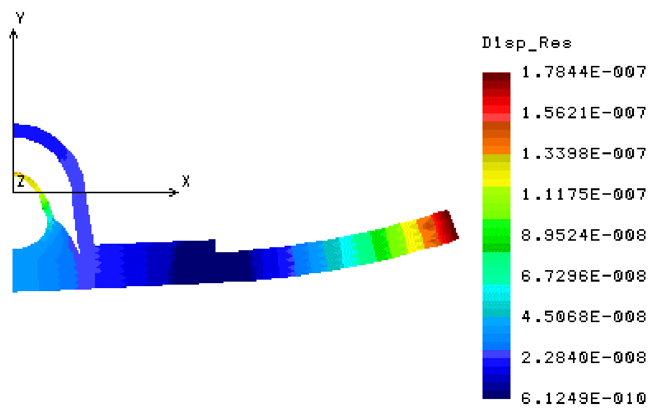

Figure 5.2-16: Static solution of stave structure with added effect of the silicon layer. Peak strain is 0.18μm, with the structure zero strain reference (Tref) of 25°C.

A possible design requirement might be to sub-cool the detector to 0°C. This increases the difference relative to the strain free state; hence, there will be an increase in this distortion. The negative CTE of the C-C starts to become evident, as shown in figure 5.2-17. Here the out-of-plane distortion peaks at 3.5μm.

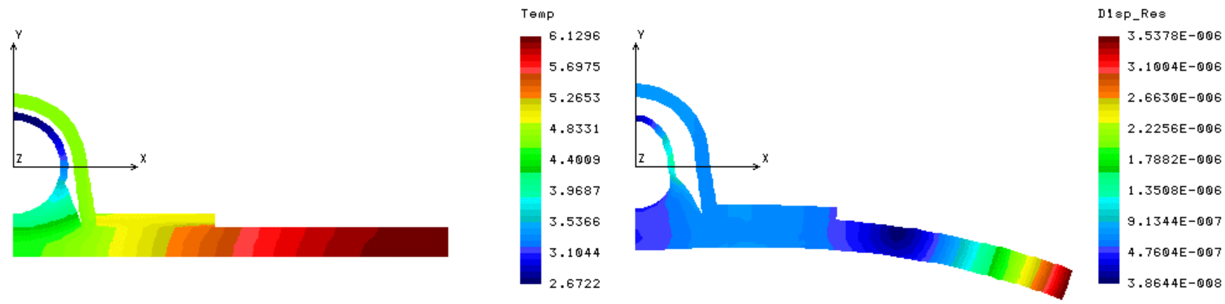

Figure 5.2-17: Module surface thermal distortions assuming 0°C entering coolant. Structure Tref=25°C.

5.2.3.4 <u>Static Solutions</u>

A FE model of the full stave was made for a 1st order approximation of the stave structural proportions. Issues that are of general interest are overall static stiffness in a gravitational field or for general handling as an isolated object, and its ability to resist thermal strains.

We assumed for the model that one end of the ladder would be fixed to the support ring at one end. At the opposite end, the ladder would be simply supported, and free to slide in the axial direction. In further studies, we would examine having both ends in a simple support.

Figure 5.2-18 depicts the sag in the ladder when subjected to 1-g normal to its module surface. All ladders are actually positioned at an angle so this solution is an extreme case. The peak displacement is 9.4µm. Several additional factors need to be considered that will increase this deflection. One, the mass of the coolant and coolant tube connections, and mass of cables and any on-board electronics must be added. If we were to assume the mass doubles, but still uniformly distributed, over that contained in the FE model we would expect the deflection to be approximately 18-20µm. When a more accurate mass distribution is established, a ladder modal analysis will be made.

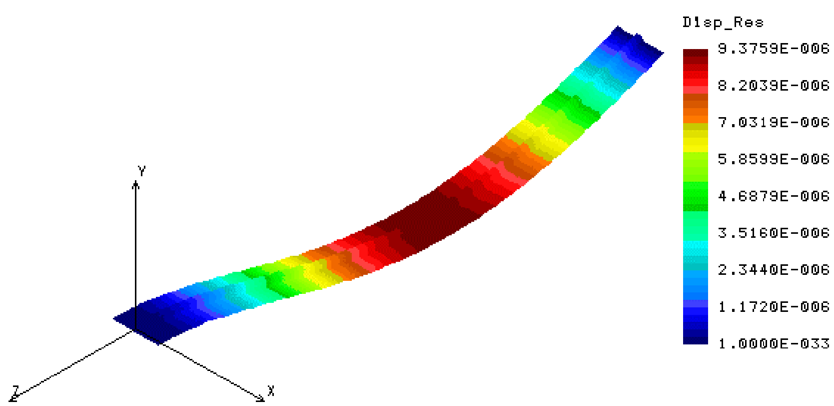

Figure 5.2-18: Gravity solution for stave with one end fixed and one simple support (RHS). Gravity vector is normal to stave thermal plane (-Y direction). Coolant tube structurally coupled to stave thermal plane.

One complication that needs to be modified in the next phase is the silicon module representation. The present FE model represents the silicon as a continuous layer, which it is not. The silicon modulus of elasticity is twice that of aluminum, and its position relative to the neutral axis of the stave cross-section creates a noticeable increase in stiffness. Consequently, our estimates of gravity effects are optimistic. The limited resources did not permit a more refined model.

An attempt was made to illustrate the effect of decoupling the cooling tube from the tube support. We propose using a rigid room temperature curing adhesive that provides this structural coupling. If the implemented design uses a flexible adhesive, as is done for structures subjected appreciable temperature changes, the result will be lower stiffness. Figure 5.2-19 is a first cut at this structural solution without the tube. We notice only a modest increase; again, this issue needs to be investigated with the decoupling of the silicon modules.

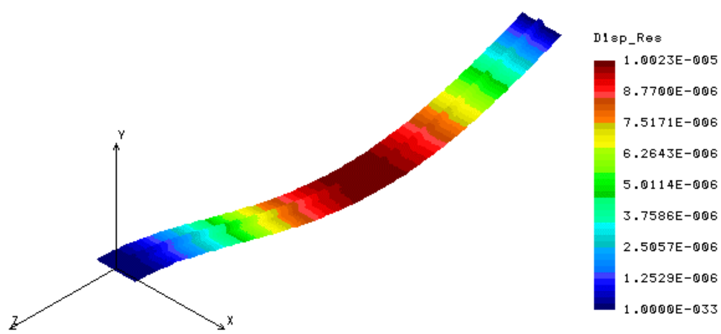

Figure 5.2-19: Gravity solution with attempt made to decouple the coolant tube from the stave structure, peak displacement of 10μm.

A thermal solution was made with this full ladder model, in spite of simplifications taken relative to the distribution of material. A slice taken from the overall model is shown in figure 5.2-20. Here we see the peak temperature is slightly over 25°C, which is fairly close to the prior estimates. We will now use this temperature distribution to calculate the thermal strain between ladder supports.

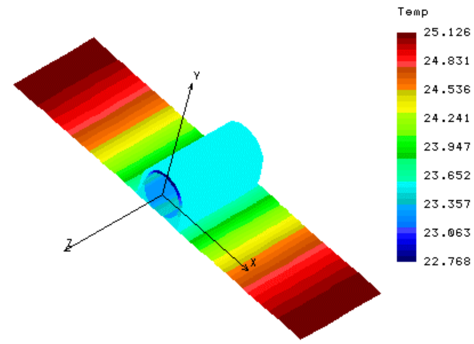

Figure 5.2-20: Thermal solution with full stave model. Temperature distribution approximates the more detailed solution illustrated in Figure 5.2-15. Peak temperature occurs at the outer edges, 25.13°C.

Figure 5.2-21 illustrates general bowing of the ladder, a peak of 6.8µm for a coolant temperature of 20°C and a surface temperature of 25.13°C. This is considered quite acceptable, but again we need to remove the effect of the coupling from the silicon modules.

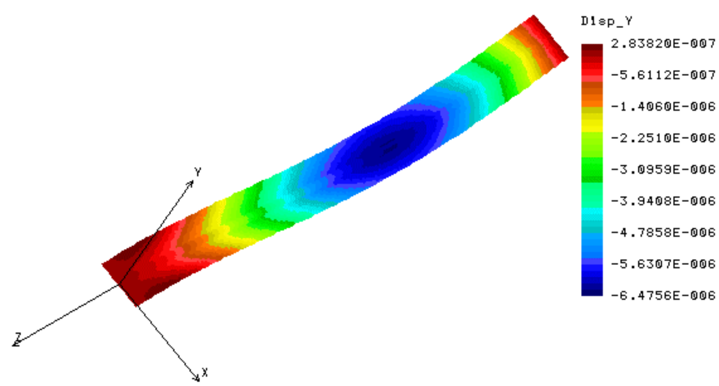

Figure 5.2-21: Thermal strain induced by stave temperature distribution shown in Figure 5.2-20. Tref= 25°C. Model based on coolant tube coupled to stave thermal plane and simple edge support on RHS, fixed edge supports on LHS.

If we were confronted with sub-cooling of the detector, the thermal strain will noticeably increase. This is illustrated in figure 5.2-22. Now the out-of-plane bowing amounts to over 80µm. It is clear that as the prospect for a sub-cooled detector is realized our need for a more exact FE model and further design studies will become far more important.

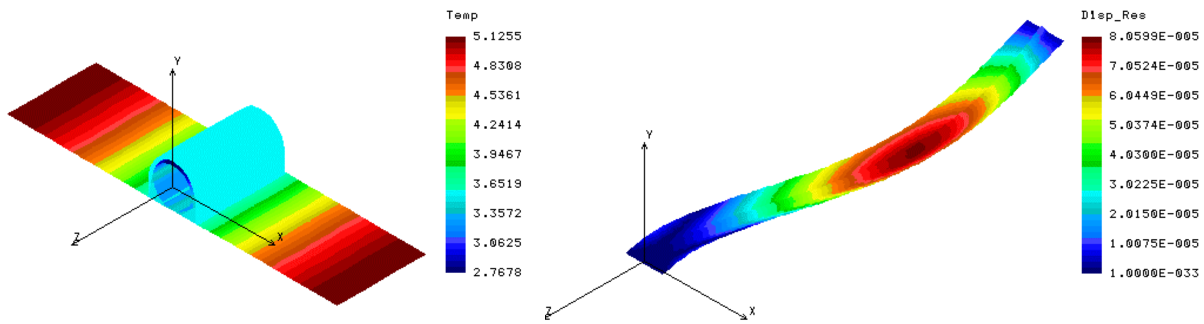

Figure 5.2-22: Thermal and thermal strain solution for full stave assuming inlet coolant temperature of 0°C and a Tref=25°C. Stave properties and support conditions remain unchanged from Figure 5.2-21.

5.2.3.5 Stave (Ladder) Radiation Length Approximation

An estimate of the radiation length was made for the stave geometry discussed in the preceding sections. The elements that comprised the material budget exclusive of the modules were:

- Composite thermal back plane onto which the modules are mounted
- Composite support for the tube, an interface between the thin-wall aluminum coolant tube and the thermal back plane
- Composite OMEGA piece, which serves to provide added stiffness
- Coolant liquid, C_5F_{12}, single phase fluid

The combined percentage radiation length is 0.7%, with the single largest contributor being the tube support (0.28%). It is anticipated a refinement to the tube support design will provide a reduction in radiation length by 0.1%; most of this gain may be lost when the penalty for adhesives is added, however. The liquid coolant radiation length, assuming a 3mm diameter tube, was 0.074%. Converting to a two-phase fluid would provide some reduction in this value. However, most of this of reduction would occur in the second stave, assuming the staves are connected in series.

6. Results Summary and Future R&D Efforts

After studying multiple concepts in both the material selection, structural, and cooling areas for the PHENIX tracker upgrade, the following recommendations for the overall concept design were found.

6.1 Material Selection Summary

6.1.1 Material Selection

- The use of GFRP sandwich composites for the base structure is suggested because of the substantial gain in the stiffness to weight ratio.

- GFRP composites also have similar RL and strength properties to carbon-carbon and beryllium, which adds to their attractiveness in this particular application.

6.1.2 Fiber Selection

Fiber selection for the GFRP composite was based on a comparison of the elastic modulus properties of several different fibers. Several candidates were selected in table 4.1-2 based upon the fibers having elastic moduli above 500 GPa.

- Since the stiffness found with every fiber candidate met the necessary stiffness requirement, fiber selection was deferred to the candidate that is most readily available and at a reasonable cost.
- M55J is the most widely used standard in the composites industry, and so it was used throughout the remainder of the structural study.

R&D for the material selection arena would be done when actual prototypes of the composite structure for the PHENIX detector are built.

6.2 Structural Analysis Summary

The structural analysis of several concepts revealed the following observations.

- Use sandwich composites for the frame structure instead of solid laminates or some combination of both. RL requirements can be met with GFRP sandwich composites, and sandwich composites have been show to have better stiffness to weight ratios.
- Outer frame structure should be a single diameter size across all three detector regions and as large a diameter as possible for the given envelope for the PHENIX Pixel Detector upgrade.
- Stability and alignment requirements can be attained with a clamshell design, if sufficient R&D is done on connection issues regarding the two clamshell halves.
- Suggest using an eight-sided shape for the outer structure. The eight-sided shape lends itself to simpler fabrication and allows for better routing of utilities out of the barrel region and end cap regions.
- Structural end disks to close out the tracker support structure are recommended for preventing deformation of the structure under dynamic load inputs at the tracker support points.

R&D includes actually building a full-scale prototype of the concept to test the dynamic and static stiffness of the structure and some small prototype tests should be done on developing the connections of the detectors to the clamshell halves and the two halves to one another. Some more development may be required with securing utilities to the structure as well.

6.3 Cooling Analysis Summary

A technical approach was defined for the support and cooling of detector modules in the End Cap and Barrel Regions of the proposed PHENIX Pixel Detector upgrade. First order calculations were made for both regions. The results of these preliminary analyses are:

6.3.1 Coolant

- Use single phase coolant, as opposed to using phase change coolants; this is suggested as a means to significantly simplify the attendant coolant system
- Use perfluorcarbon fluid, C_5F_{12} or C_6F_{14}, with the final decision reserved for the final system study
- Flow coolant under turbulent flow conditions to enhance convective heat transfer coefficients, thereby substantially reducing the temperature drop in the coolant film and the gradient in the detector support structures
- Supply the coolant at 20°C inlet, unless sub-cooling of the overall detector is required.

6.3.2 End Cap Region

- Use a flat conical panel sandwich structure for supporting the modules, with module mounting alternating front to back on adjacent panels. Panels are termed sectors, with cooling provided to two adjacent sectors in series. Series connection of adjacent sectors provides modularity of two. Higher modularity may weaken the detector reliability in the event of an isolated failure of a cooling component.
- Construct the structure as a half conical structure, mounted to an outer clamshell sandwich structure.
- Cooling of the End Cap sectors requires removal of nominally 15W per sector, at a comparatively low heat flux. A 2mm inner tube diameter is suggested with a mass flow rate of 9.8g/s for a pressure drop of 6psi per sector. Resulting peak temperature in the surface of the sector should be on the order of 4.5°C or less. Bulk fluid temperature rise for two sectors would on the order of 3°C. Pressure drop can be reduced to under 1psi by using a 3mm diameter cooling tube.
- The preliminary sandwich spacing used in the thermostructural solution was 2mm, with the void between cooling channels filled with carbon foam. The cooling channel is sandwiched between two thermally conductive facings. The facings were assumed carbon-carbon material for reasons of high thermal conductivity and structural stiffness

Further studies of the end cap clamshell panels are suggested for refining the composite sandwich design and to assess thermal strains. However, the thermal strains can be minimized by using a stiff composite sandwich structure.

6.3.3 Barrel Region

In the Barrel Region, we chose to analyze the ladder concept for the silicon strip layer since the total heat load per ladder is greater, 27W versus ~8W per ladder for the pixel layer. The next step in the study will include the pixel ladder design.

Continuing the listing of findings and suggestions:

- Use a ladder, or stave, concept supported at its ends by composite rings.
- One end of the ladder would emulate a simple support and the other a fixed end support. These boundary conditions were chosen to minimize thermal strains.

- Suggested stave structure comprises a C-C thermal plane for mounting pixel modules, or silicon strip detectors. To add stiffness to the long flat surface, a thin, 0.4mm OMEGA shaped composite is bonded to the back of the thermal plane.
- Cooling tube is bonded to the back of the C-C thermal plane with a C-C tube support, using a rigid room temperature adhesive
- Use an Aluminum cooling tube 3mm in diameter supplied with a 23g/s single-phase perfluorocarbon fluid, e.g., C_5F_{12}, layer 3 or 4. Estimated bulk fluid temperature rise is 1.1°C for 27W per stave heat pick up. Corresponding pressure drop is approximately 1psi per stave. Estimated peak temperature for a silicon layer (3 or 4) is 8.6°C. Analysis is required for the pixel layer; temperatures may be somewhat higher due to the higher localized heat flux, 0.7W/cm^2 versus 0.35W/cm^2 for the silicon strip layer.
- Preliminary estimate of bowing for the silicon strip layer, along its 30cm longitudinal axis, due to thermally induced strains is modest. This assumes the coolant is supplied at 20°C. If detector sub-cooling to 0° C is required, the thermally induced strain would increase to 80µm. This thermal component strain for a pixel layer stave, with its higher localized heat flux, may be greater.

Overall, we feel the system parameters and design approach selected for consideration by the PHENIX collaboration reflects a conservative design with a focus on simplicity to hold R&D and acquisition costs down. The basic structural concepts chosen for supporting the pixel modules are expected to stay within or close to the specified radiation length budget.

7. Design Costs and Manpower Requirements

Table 7.1-1 contains a very rough order of magnitude idea of what costs might be to develop the following structural and cooling concepts of the PHENIX tracker into deliverable hardware. The numbers listed contain both labor and hardware, and they are based upon some historical information from development costs involved with ATLAS[4] and SSC programs and some general educated guesses. The major difficulty with developing these estimates is that they are highly dependent on the direction and focus of the concepts and all other hardware that interfaces with them. As the detector electronics, detectors, electromagnetic enclosure, etc. all develop, they could all have a major impact on the development of the structural and cooling concepts to where these initial estimates would be grossly incorrect. With that said, the information listed in table 7.1-1 is to be taken as preliminary in all cases. Manpower estimates would be about 2.0-2.5 FTE's for the duration of the work involved with developing the design.

Table 7.1-1: Manpower and Hardware Cost Estimates for the PHENIX Pixel/Silicon Upgrade.

Item	Engr R&D ($K)	Design ($K)	Mfg Liaison ($K)	Tooling ($K)	Fabrication ($K)	Materials ($K)	Total ($K)
Coolant Circulation and Refrigeration System		50	10			25	85
Outer Structure (2 pieces)	50	35	10	45	50	20	210
End Cap Disks (16 pieces), plus cooling tubes	75	35	25	35	50	20	240
Disk Mounts (64 pieces)	10	15	5	5	15	5	55
Barrel Ladder Staves (~58 pieces)	50	50	20	20	58	20	218
Ladder Support Structure (4 pieces)		45	10	20	25	10	110
Ladder Coolant Tubes (~58 tubes), plus terminations	10	10	2	5	15	5	47
Total	195	240	82	130	213	105	965

8. References

1. Miller, W.O., et. Al., *Superconducting Super Collider Silicon Tracking Subsystem Research and Development*, LA-12029, 1990.
2. Lee, D., et. Al., *Specifications for PHENIX Silicon/Pixel Tracker Conceptual Design*, LANL, Sept 2002.
3. Rohsenow, W.M., *Handbook of Heat Transfer Fundamentals*, 2nd Edition, McGraw-Hill.
4. Miller, W.O., *Atlas Pixel Detector Global Supports and Disk Support Ring Cost Book*, Unreleased HYTEC document prepared for DOE Review and supplied to Lawrence Berkeley National Laboratory.